Journal of Superconductivity and Novel Magnetism (2022) 35:473–483
https://doi.org/10.1007/s10948-021-06085-5

ORIGINAL PAPER

Sol–Gel Auto-combustion Preparation of $M^{2+} = Mg^{2+}$, Mn^{2+}, Cd^{2+} Substituted $M_{0.25}Ni_{0.15}Cu_{0.25}Co_{0.35}Fe_2O_4$ Ferrites and Their Characterizations

Asma Aslam[1] · Atta Ur Rehman[1] · Nasir Amin[1] · Mongi Amami[2,3] · M. Ajaz un Nabi[1] · Hussein Alrobei[4] · M. Asghar[5] · N. A. Morley[6] · Maria Akhtar[1] · Muhammad Imran Arshad[1] · Mudassar Maraj[7] · Kamran Abbas[8]

Received: 2 August 2021 / Accepted: 3 November 2021 / Published online: 13 November 2021

Abstract

Cost-effective and controllable synthesis of $M_{0.25}Ni_{0.15}Cu_{0.25}Co_{0.35}Fe_2O_4$ ($M^{2+} = Mg^{2+}$, Mn^{2+}, and Cd^{2+}) ferrites via the sol–gel auto-combustion technique. The impact of divalent cations on the structural, dielectric, and optoelectrical properties of ferrites was examined by XRD, FTIR, Raman, LCR, UV–Vis, and two probe I-V measurement techniques. The crystallite size was 52.66 nm, and the minimum specific surface area was observed 5.1507 m^2/g for Mg^{2+} doped NCCF ferrite. The FTIR and Raman analysis also confirmed the substitution of divalent cations ($M^{2+} = Mg^{2+}$, Mn^{2+}, and Cd^{2+}) at their respective lattice sites. The maximum energy bandgap was 1.67 eV Mg^{2+}-doped NCCF ferrite as compared to other divalent ion-doped ferrites. The dielectric loss decreased while the ac conductivity increased with increasing frequency, and the minimum values were observed for Mg^{2+}-doped NCCF ferrite. The activation energy was observed maximum for Mg^{2+}-doped NCCF ferrite (0.2234 eV). Due to incredible properties including small specific surface area, large energy band gap, high resistivity, and loss dielectric loss of Mg^{2+}-doped NCCF ferrite have potential applications in different fields.

Keywords Divalent · Specific surface area · Energy band · Raman · Activation energy

✉ Muhammad Imran Arshad
miarshadgcuf@gmail.com

1 Department of Physics, Government College University, Faisalabad 38000, Pakistan

2 Department of Chemistry College of Sciences, King khalid university, P.O. Box 9004, Abha, Saudi Arabia

3 Laboratoire Des Matériaux Et de L'environnement Pour Le Développement Durable LR18ES10, 9 Avenue Dr. Zoheir SAFI, 1006 Tunis, Tunisia

4 Department of Mechanical Engineering, College of Engineering, Prince Sattam Bin Abdulaziz University, Al Kharj, Saudi Arabia

5 Controller of Examination, National Skills University, Islamabad, Pakistan

6 Department of Materials Science and Engineering, The University of Sheffield, Sheffield S1 3JD, UK

7 Research Center for Optoelectronic Materials and Devices, School of Physical Science and Technology, Guangxi University, Nanning 530004, China

8 Department of Mechanical Engineering, College of Engineering, Taif University, P.O. Box 1109, Taif 21944, Saudi Arabia

1 Introduction

Nanoparticles of spinel ferrites are widely used in the latest technology as telecommunications [1], usage of wastewater and photocatalytic water splitting [2–4], electronics [5], and magnetic recordings [6]. AB_2O_4 is the general formula of the soft spinel ferrites in which B^{3+} represent trivalent elements occupying octahedral sites while A^{2+} represent divalent elements occupying tetrahedral site [7]. The chemical composition, cation distribution, doping ratio with significant parameters like synthesis technique, and grain morphology affected the optoelectrical, structural, and magnetic parameters of the spinel ferrites [8]. In the electronics growth industry, such remarkable change in the electromagnetic properties of the ferrites makes them the most significant for use in advanced research applications [9, 10].

Warsi et al. [11] prepared Erbium-doped Ni-Co spinel ferrite by using the co-precipitation technique. Two probe IV techniques were used to find the electrical resistivity of the prepared ferrites, and it was found 6.02×10^7 Ω cm. Almessiere et al. [12] studied $Ni_{0.3}Cu_{0.3}Zn_{0.4}Fe_2O_4$ synthesized by ultrasonic irradiation method. At 350 K, the

maximum ac conductivity for $x = 0.02$. Sadaqat et al. [13] reported Tb^{3+} substituted cobalt ferrite prepared by using the sonochemical procedure in which the lattice constant declined with the addition of Tb^{3+}. Almessiere et al. [14] reported Dy^{3+} replaced $Mn_{0.5}Zn_{0.5}Fe_{2-x}O_4$ ferrites synthesized by the ultrasonic irradiation process in which the energy band gap declined calculated by using the Tauc equation. Slimani et al. [15] synthesized Ni-Cu–Zn nanoparticles by the sonochemical process in which the reaction time declined which minimized the requirement of a large number of organic solvents. At 393 K, the ac conductivity is minimum for $x = 0.02$.

Various techniques are used to synthesize the nanoparticles, co-precipitation [16–21], auto combustion sol–gel techniques [22], reverse micelle technique [23], and solid-state reaction [24]. Because of the fine surface morphology, low-temperature preparation, and greater particle homogeneity, the sol–gel auto combustion approach was shown to be better [22, 25]. In this research work, we synthesized $M_{0.25}Ni_{0.15}Cu_{0.25}Co_{0.35}Fe_2O_4$ ($M^{2+} = Mg^{2+}$, Mn^{2+}, and Cd^{2+}) via the sol–gel auto-combustion technique. The effects of divalent metal Mg^{2+}, Mn^{2+}, and Cd^{2+} ions on the optoelectrical, dielectric, and structural parameters of the $M_{0.25}Ni_{0.15}Cu_{0.25}Co_{0.35}Fe_2O_4$ ferrite ferrites are discussed in this article and observed how it changed the structural parameters and electrical resistivity of the prepared ferrites.

2 Experimental Details

2.1 Materials and Method

$M_{0.25}Ni_{0.15}Cu_{0.25}Co_{0.35}Fe_2O_4$ ferrites doped with divalent metal Mg^{2+}, Mn^{2+}, and Cd^{2+} ions (*M^{2+} doped NCCF ferrites*) were synthesized by auto-combustion sol–gel technique. All the following chemicals [Cu $(NO_3)_2{\cdot}3H_2O$], [Cd $(NO_3)_2{\cdot}4H_2O$], [Mg $(NO_3)_2{\cdot}6H_2O$], [Mn $(NO_3)_2{\cdot}4H_2O$], [Ni $(NO_3)_2{\cdot}6H_2O$], [Co $(NO_3)_2{\cdot}6H_2O$], [Fe $(NO_3)_3{\cdot}9H_2O$] and citric acid were measured according to stoichiometry and dissolved into distilled water separately on a magnetic stirrer with continuously stirring. All the dissolved chemicals were poured into a beaker to get a homogeneous solution through stirring. Ammonia was added drop-wise into the solution to achieve a pH = 7. After maintaining pH, the solution was stirred at 80 °C to form a gel which was further converted into ash and sintered at 800 °C for 8 h. The fine powder of sintered ash was obtained through grinding, and pellets of 7 mm were made by using a hydraulic press.

2.2 Characterization Used

For structural analysis and phase confirmation, a Bruker D8 Advance X-ray diffractometer (XRD) with a Copper K_α source ($\lambda = 1.54$ Å) was employed. The absorption bands were studied using Fourier transform infrared (FTIR) spectroscopy. UV–visible spectroscopy was used to determine the energy bandgap (E_g). To evaluate electrical resistivity, a Keithley Electrometer Model 2401 was used for current–voltage (I–V) measurements. For dielectric measurements, the IM3536 series LCR Meter was employed.

3 Results and Discussion

3.1 XRD Analysis

The structural properties of the as-prepared ferrites were studied through the XRD analysis. Figure 1 indicates the XRD patterns of the as-prepared ferrites and planes (220), (311), (400), (422), and (511) were labeled which established the development of their cubic spinel matrix. Bragg's law was utilized to calculate the inter planer distance of the as-prepared ferrites [26]:

$$d = \frac{n\lambda}{2sin\theta} \tag{1}$$

where θ is Braggs' angle and λ is 1.5046 Å while $n = 1$. It was observed that the inter planer distance of the M^{2+} doped NCCF ferrites lies in the range of 2.5226–2.5333 Å (as seen in Table 1). The Scherrer's formula (2) was employed to find the crystallite size of the prepared ferrites and given as [26, 27]:

$$D = \frac{n\lambda}{\beta Cos\theta} \tag{2}$$

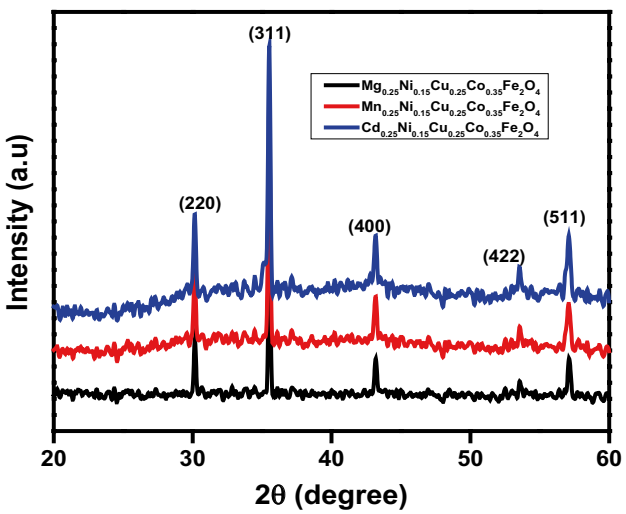

Fig. 1 XRD patterns of M^{2+}-doped NCCF ferrites

Table 1 Structural parameters of the as-prepared ferrites

Lattice parameter	Mg^{2+}-doped NCCF	Mn^{2+}-doped NCCF	Cd^{2+} -doped NCCF
d (Å)	2.5226	2.5273	2.5333
a_{exp} (Å)	8.3664	8.3821	8.4021
D (nm)	52.66	47.26	22.35
ρ_X(g/cm^3)	5.1507	5.2969	5.5812
ρ_b(g/cm^3)	2.9330	2.9684	2.9839
P %	43.05	43.95	46.53
$F(\theta)$ (radian)	2.9486	2.9553	2.9637
p (%)	20.87	18.70	8.82
(ε)	0.1572	0.1566	0.1558
δ (g/m^3)	0.0054	0.0059	0.0124
S (m^2/g)	5.1507	5.2969	5.5812
L_A (Å)	3.6228	3.6296	3.6382
L_B (Å)	2.9579	2.9635	2.9706

where n is a constant which is 0.94, β is FWHM, and θ is the angle of diffraction. The following formula (3) [28] was used to find the experimental lattice constant of the M^{2+} doped NCCF ferrites:

$$a_{exp} = d_{hkl}\sqrt{h^2 + k^2 + l^2} \tag{3}$$

where (h k l) represents the miller indices of and "a" is the experimental lattice constant of the prepared ferrites. Equation (4) was employed to estimate the X-ray density of the prepared ferrites and given as [28]:

$$\rho_X = \frac{8M}{N_A a_{exp}^3} \tag{4}$$

where M is the molar mass of the prepared ferrites, and N_A are the Avogadro's number (6.022×10^{23} mol^{-1}). It is observed that the lattice constant increased in the range of 8.3664–8.4021 Å due to the addition of dopant Mg^{2+}, Mn^{2+}, and Cd^{2+} ions in the NCCF ferrites. The crystallite size of the M^{2+} doped NCCF ferrites decreased in the range of 52.66–22.35 nm. It was found from Table 1 that the minimum crystallite size was 22.35 nm for the Cd^{2+}-doped NCCF ferrite. Such remarkable change raised due to substitution of large ionic radii divalent ions Mg^{2+} (0.72 Å), Mn^{2+} (0.66 Å), and Cd^{2+} (0.78 Å) with Fe^{3+} (0.645 Å). The X-ray density of the as-prepared ferrites increased from 5.1507 g/cm^3 to 5.5812 g/cm^3. The bulk density of the prepared ferrites is calculated by using the given formula [29]:

$$\rho_b = \frac{Mass}{Volume} = \frac{M}{\pi r^2 \times h} \tag{5}$$

Here, "M" is the mass of the pellet while "h" and "r" are the thickness and radius of the pellet respectively, and given in Table 1. The porosity percentage was estimated via the following formula [29]

$$P\% = [1 - \frac{\rho_b}{\rho_x}] \times 100 \tag{6}$$

Here, ρ_b and ρ_X are the bulk density and X-ray density of the M^{2+}-doped NCCF ferrites. The difference in the values of ρ_b and ρ_X observed due to the existence of some pores which develop in the sintering process [30]. X-ray density and the molar mass of the prepared ferrites are directly proportional to each other so ρ_X increased while ρ_b increased due to addition of divalent metal Mg^{2+}, Mn^{2+}, and Cd^{2+} content into the prepared ferrites. The porosity percentage of the M^{2+}-doped NCCF ferrites increased from 43.03 to 46.53% and is tabulated in Table 1.

The experimental lattice constant was confirmed by the Nelson–Riley function which is given as [28]

$$F(\theta) = \frac{1}{2}[\frac{Cos^2\theta}{Sin\theta}] + \frac{Cos^2\theta}{\theta} \tag{7}$$

The values of the Nelson–Riley function demonstrate it is in good agreement with the calculated values of the experimental lattice constant (as seen in Table 1). Different lattice parameters such as strain (ε), dislocation density (δ), specific surface area (S), and packing factor (p) percentage are calculated through given formulas [28]:

$$\varepsilon = \frac{1}{d^2} \tag{8}$$

$$\delta = \frac{15\varepsilon}{a_{exp} D} \tag{9}$$

$$S = \frac{6000}{\rho_{X \times D}} \tag{10}$$

Table 2 Cation distribution and theoretical of M^{2+}-doped NCCF ferrites

Tetrahedral site	Octahedral site	r_A (Å)	r_B (Å)	a_{th} (Å)
$[Mg_{0.0125}Ni_{0.015}Cu_{0.0375}Co_{0.07}Fe_{0.865}O_4]_A$	$[Mg_{0.2375}Ni_{0.135}Cu_{0.2125}Co_{0.28}Fe_{1.135}O_4]_B$	0.5985	0.6854	8.3015
$[Mn_{0.2}Ni_{0.015}Cu_{0.0375}Co_{0.07}Fe_{0.6775}O_4]_A$	$[Mn_{0.05}Ni_{0.135}Cu_{0.2125}Co_{0.28}Fe_{1.3225}O_4]_B$	0.6108	0.6768	8.2975
$[Cd_{0.25}Ni_{0.015}Cu_{0.0375}Co_{0.07}Fe_{0.6275}O_4]_A$	$[Ni_{0.15}Cu_{0.25}Co_{0.35}Fe_2O_4]_B$	0.6438	0.6773	8.3496

Table 3 Oxygen ion parameter, tolerance factor, bond lengths, and bond edge lengths of M^{2+}-doped NCCF ferrites

Ferrites	*U*	*T*	Bond lengths		Bond edge lengths		
			R_A (Å)	R_B (Å)	d_{AL} (Å)	d_{BL} (Å)	d_{BLU} (Å)
Mg^{2+}-doped NCCF	0.3824	1.0388	1.9186	2.1553	1.9185	2.0316	2.9605
Mn^{2+}-doped NCCF	0.3829	1.0416	1.9295	2.1638	1.9308	2.0307	2.9665
Cd^{2+}-doped NCCF	0.3849	1.0429	1.9632	2.1868	1.9638	2.0204	2.9752

$$p = \frac{D}{d} \tag{11}$$

Here, a_{exp}, D, d, and ρ_X are the experimental lattice constant, crystallite size, inter planer distance, and X-ray density respectively. The strain and packing factor percentage were reduced while the dislocation density and specific surface area were increased with the substitution of dopant ions as seen in Table 1. Hopping lengths L_A and L_B are calculated by using the given formulas [28, 31]:

$$L_A = \frac{a_{exp}\sqrt{3}}{4} \tag{12}$$

$$L_B = \frac{a_{exp}\sqrt{2}}{4} \tag{13}$$

where L_A and L_B are hopping lengths of tetrahedral and octahedral sites respectively. L_A is the distance between cation and oxygen ion at tetrahedral site while L_B is the distance between cation and oxygen ion at octahedral site. The calculated values of L_A and L_B are reported in Table 1. M^{2+}-doped NCCF ferrites have mixed spinel structure because Cu^{2+}, Co^{2+}, Mg^{2+}, Ni^{2+}, and $Fe^{2+/3+}$ ions prefer both A-site (tetrahedral) and B-site (octahedral) while Cd^{2+} ions prefer only tetrahedral sites [32–36]. The cation distribution of the as-prepared ferrites is determined by $[M^{2+}{}_{1-x}\ T^{3+}{}_{x}]_A\ [M^{2+}{}_{x}\ T^{3+}{}_{2-x}]_B\ O_4$ which are given in Table 2 while the ionic radii are calculated by using following formulas:

Table 4 Interionic distance of the as-prepared M^{2+}-doped NCCF ferrites

Bond lengths (Å)	Mg^{2+}-doped NCCF	Mn^{2+}-doped NCCF	Cd^{2+}-doped NCCF
b	2.9575	2.9631	2.9701
c	3.4685	3.4750	3.4833
d	3.6226	3.6295	3.6381
e	5.4339	5.4442	5.4572
f	5.1232	5.1328	5.1450
p	0.9749	0.9668	0.9499
q	3.7454	3.7697	3.8119
r	7.1721	7.2186	7.2994
s	4.2673	4.2811	4.3024

$$r_A = C_{AM} r\left(M^{2+}\right) + C_{ANi} r\left(Ni^{2+}\right) + C_{ACu} r\left(Cu^{2+}\right) + C_{ACo} r\left(Co^{2+}\right) + C_{AFe} r\left(Fe^{2+}\right) \tag{14}$$

$$r_B = \frac{1}{2}[C_{BM} r\left(M^{2+}\right) + C_{BNi} r\left(Ni^{2+}\right) + C_{BCu} r\left(Cu^{2+}\right) + C_{BCo} r\left(Co^{2+}\right) + C_{BLa} r\left(La^{3+}\right) + C_{BFe} r\left(Fe^{2+}\right)] \tag{15}$$

where $r(Cd^{2+})$, $r(Ni^{2+})$, $r(Cu^{2+})$, $r(Co^{2+})$, and $r(Fe^{2+})$ are the ionic radii while C_{Cd}, C_{Ni}, C_{Cu}, C_{Co}, and C_{Fe}r are the concentration of Cd^{2+}, Ni^{2+}, Cu^{2+}, Co^{2+}, and Fe^{3+}, respectively. The calculated values of r_A and r_B changed due to addition of divalent metal Mg^{2+}, Mn^{2+}, and Cd^{2+} in the prepared ferrites which are given in Table 2.

The theoretical lattice constant of the M^{2+}-doped NCCF ferrites are calculated by using the formula [28]

$$a_{th} = \frac{8}{\sqrt[3]{3}}[(r_A + R_o) + \sqrt{3}(r_B + R_o)] \tag{16}$$

where r_A, r_B is the ionic radii of A and B-site of the sublattice while $R_o = 1.32$ Å is the oxygen ion radius [28]. The theoretical lattice constant is tabulated in Table 2 and lies in the range 8.2975–8.3496 Å due to doping of Mg^{2+} (0.72 Å), Mn^{2+} (0.66 Å), and Cd^{2+} (0.78 Å) ions into the NCCF lattice. A small difference between theoretical and experimental lattice constant is because of the cation distribution of

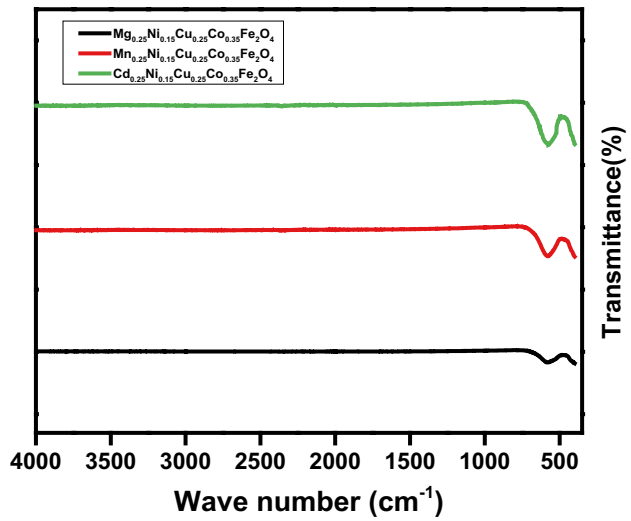

Fig. 2 FTIR spectra of M^{2+}-doped NCCF ferrites

Table 5 Absorption bands and force constants of M^{2+}-doped NCCF ferrites

Ferrites	v_T(cm^{-1})	$K_T\times10^5$ (dyne/cm^{-1})	v_O(cm^{-1})	$K_o\times10^5$ (dyne/cm^{-1})	E_g (eV)
Mg^{2+}-doped NCCF	585.21	3.1675	421.26	1.6413	1.67
Mn^{2+}-doped NCCF	575.48	3.0630	422.11	1.6480	1.25
Cd^{2+}-doped NCCF	579.80	3.1092	433.43	1.7375	0.85

the anions and cations in the spinel structure. The tolerance factor is calculated using the given formula [28]:

$$T = \frac{1}{\sqrt{3}}\left(\frac{rA + Ro}{rB + Ro}\right) + \frac{1}{\sqrt{2}}\left(\frac{Ro}{rB + Ro}\right) \tag{17}$$

where r_A, r_B, R_o (1.32 Å) are the ionic radii of A-site, B-site, and oxygen ion respectively. The tolerance factor is close to one which indicates the development of the spinel matrix because the tolerance factor is 1 for a perfect spinel matrix [16]. The oxygen ion parameter of the prepared ferrites is calculated by using the given formula [28]:

$$U = (r_A + R_o)\frac{1}{\sqrt{3a}} + \frac{1}{4} \tag{18}$$

The oxygen ion parameter has an ideal value of 0.375 [16]. The chemical composition of the material, synthesis technique, and sintering of the prepared ferrites may affect the oxygen ion parameter from its ideal value [16]. The calculated values of "*U*" are tabulated in Table 3. The smallest distance between A-site (tetrahedral) and oxygen ion is known as tetrahedral bond length (R_A) while the shortest distance between B-site and oxygen ion is known as octahedral

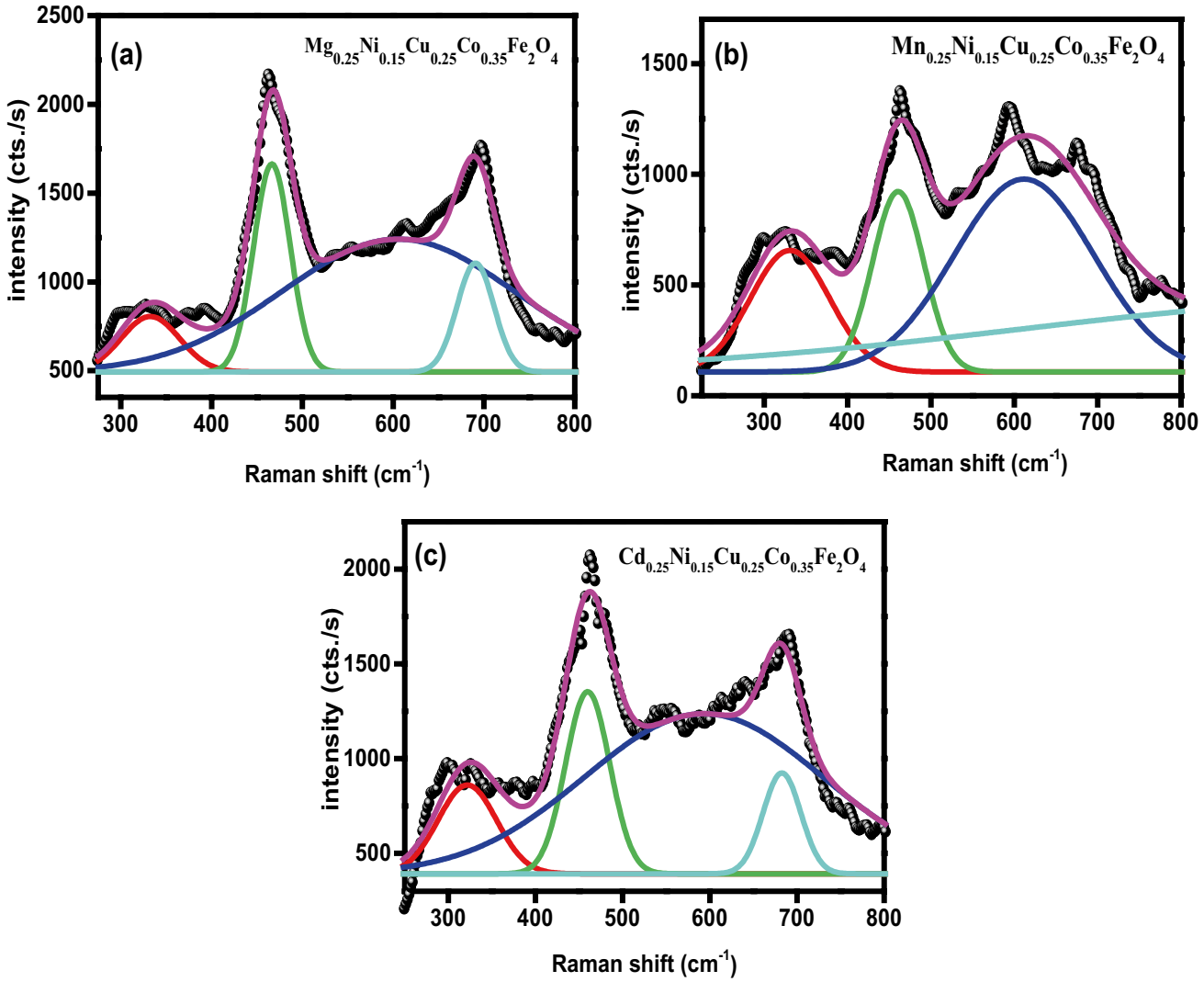

Fig. 3 Raman peaks of M^{2+}-doped NCCF ferrites

Table 6 Raman peaks for tetrahedral and octahedral sites of M^{2+}-doped NCCF ferrites

Ferrites	E_g (cm^{-1})	T_{2g} (2) (cm^{-1})	T_{2g} (3) (cm^{-1})	A_{1g} (1) (cm^{-1})	A_{1g} (2) (cm^{-1})
Mg^{2+}-doped NCCF	296	461	534	614	695
Mn^{2+}-doped NCCF	299	462	531	611	694
Cd^{2+}-doped NCCF	300	462	531	612	693

bond length (R_B). Equations (19) and (20) were utilized to determine the tetrahedral and octahedral bond lengths of the prepared ferrites respectively and reported in Table 3.

$$R_A = \alpha_{exp}\sqrt{3}(\delta + \frac{1}{8}) \tag{19}$$

$$R_B = \alpha_{exp}\sqrt{(\frac{1}{16} + \frac{\delta}{2} + 3\delta^2)} \tag{20}$$

Here, α_{exp} is the experimental lattice constant, and δ is known as the inversion parameter which is equal to U-U_{ideal}. It is observed that both bond lengths increased due to the addition of dopant divalent metal (Mg^{2+}, Mn^{2+}, and Cd^{2+}). Equations (21), (22), and (23) are used to determine the octahedral shared edge length d_{BL}, octahedral unshared edge length d_{BLU}, and tetrahedral edge length d_{AL} of the prepared ferrites and reported in Table 3:

$$d_{BL} = \sqrt{2}\left(2U - \frac{1}{2}\right)\alpha_{exp} \tag{21}$$

$$d_{BLU} = \left(\sqrt{4U^2 - 3U + \frac{11}{16}}\right)\alpha_{exp} \tag{22}$$

$$d_{AL} = \sqrt{2}\left(2U - \frac{1}{2}\right)\alpha_{exp} \tag{23}$$

Here, U is the oxygen ion parameter, and α_{exp} is the experimental lattice constant. The interionic distance was determined using relations (24) and (25) [28]:

Metal and metal interaction (cation-cation):

$$b = \left(\frac{\alpha_{exp}}{4}\right)\sqrt{2}, c = \left(\frac{\alpha_{exp}}{8}\right)\sqrt{11}, d = \left(\frac{\alpha_{exp}}{4}\right)\sqrt{3},$$
$$e = \left(\frac{3\alpha_{exp}}{8}\right)\sqrt{3}, f = \left(\frac{\alpha_{exp}}{4}\right)\sqrt{6} \tag{24}$$

M–O interaction (cation- anion):

$$p = \alpha_{exp}\left(\frac{5}{8} - U\right), q = \left(U - \frac{1}{8}\right)\sqrt{3},$$
$$r = \alpha_{exp}\left(U - \frac{1}{8}\right)\sqrt{11}, s = \frac{\alpha_{exp}}{3}\left(U + \frac{1}{2}\right)\sqrt{3} \tag{25}$$

The interionic distance explains the magnetic interaction between M–O (p-s) and M–M (b-f) due to the addition of dopant Mg^{2+}, Mn^{2+}, and Cd^{2+} ions in the prepared ferrites. The trend of interionic distances increased and decreased between M–M and M–O interaction is given in Table 4.

3.2 FTIR Analysis

The absorption bands of M^{2+} doped NCCF ferrites were studied by the FTIR spectra. Figure 2 indicates

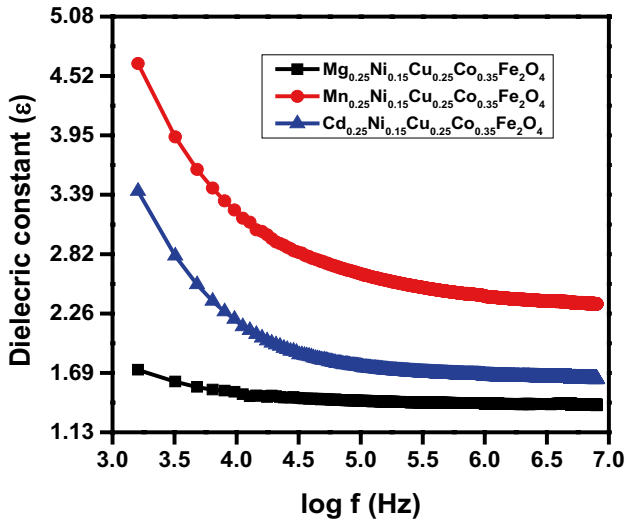

Fig. 4 Dielectric constant and frequency function of M^{2+}-doped NCCF ferrites

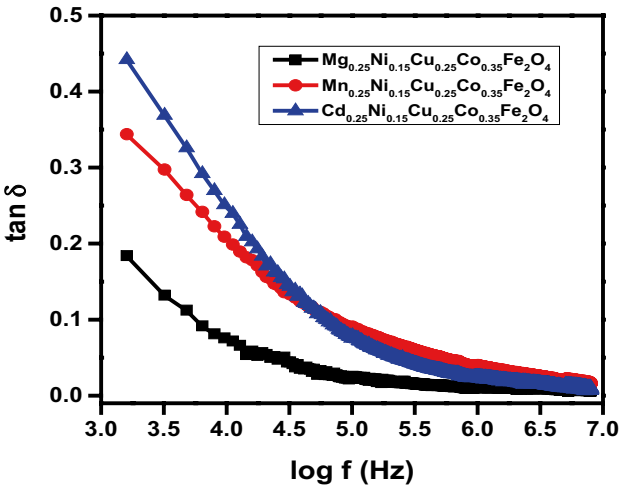

Fig. 5 Dielectric loss and frequency function of M^{2+}-doped NCCF ferrites

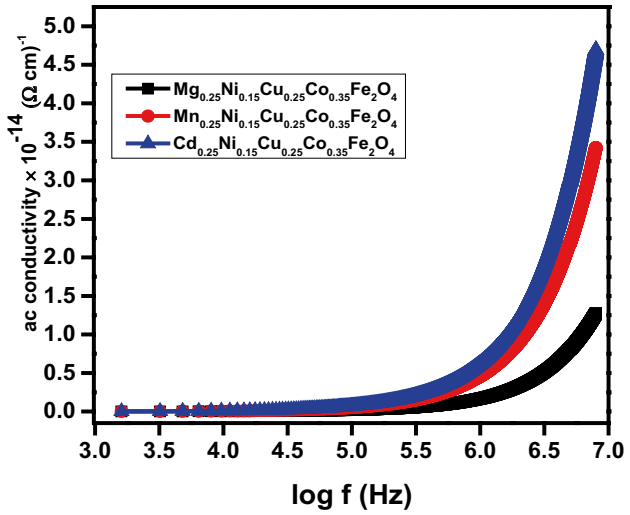

Fig. 6 Ac conductivity and frequency function of M^{2+}-doped NCCF ferrites

the spectra of FTIR which was observed in the range of 400–4000 cm^{-1}. The lower frequency absorption band (v_O) at octahedral site recorded in the range of 421.26–433.43 cm^{-1} (Table 5) which also endorses the development of the single-phase spinel cubic structure while high-frequency absorption band (v_T) at tetrahedral site recorded in the range of 575.48–585.21 cm^{-1} (Table 5) for all the as-prepared ferrites which also confirm the existence of M–O bond at the tetrahedral site [16].

3.3 Raman Analysis

Raman spectroscopy was used to investigate the vibrational and structural characteristics of M^{2+} doped NCCF ferrites. Figure 3 elaborates the five Raman modes of the as-prepared ferrites which changed with the addition of divalent metal ions (Mg^{2+}, Mn^{2+}, and Cd^{2+}). All the peaks of Raman mods are listed in Table 6 which are observed in the range of 200–850 cm^{-1}. Raman modes observed at low frequency (less than 500 cm^{-1}) and high-frequency mode (more than 500 cm^{-1}) belong to the octahedral site and tetrahedral site of phonon vibrations respectively which also confirm the cation distribution due to the addition of the dopant divalent metal Mg^{2+}, Mn^{2+}, and Cd^{2+} ions into the prepared ferrites [37, 38].

3.4 Dielectric Analysis

The dielectric characteristics of the prepared ferrites were analyzed by LCR meter in the pellet form having a diameter of 7 mm. The effect of dopant divalent (Mg^{2+}, Mn^{2+}, Cd^{2+}) metal ions on the dielectric characteristic of the prepared ferrites was recorded in the frequency range of 4 Hz to 8 MHz. Figure 4 indicates the dielectric constant as a frequency function of M^{2+}-doped NCCF ferrites. It is observed that the dielectric constant has an inverse relation with frequency as frequency increased, the dielectric constant decreases. This result is ascribed by a slowdown in electron hopping which reduced polarization as frequency increased because the prepared ferrites show no response to the applied external field at a high-frequency range [39, 40]. Koops and Maxwell–Wagner model [41] was used to elaborate the slowdown of hopping electrons at grain boundaries which decreased the dielectric constant at high frequencies. Figure 5 indicates the decrease in dielectric loss of M^{2+} doped NCCF ferrites due to the addition of divalent metal ions into the M^{2+}-doped NCCF ferrites. Figure 6 reveals the ac conductivity of M^{2+}-doped NCCF ferrites at a

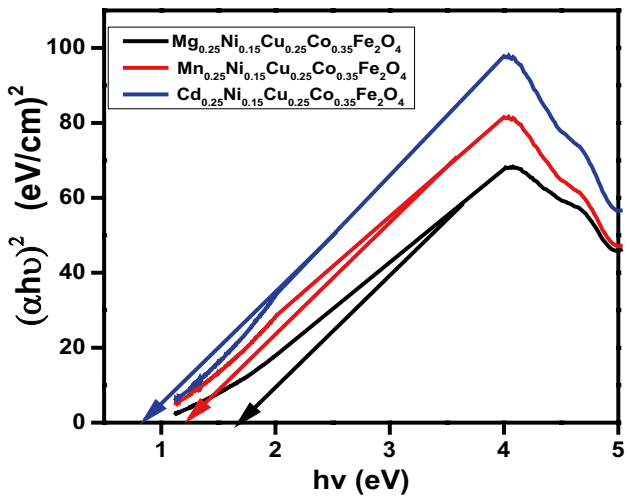

Fig. 7 Optical band gap of M^{2+}-doped NCCF ferrites

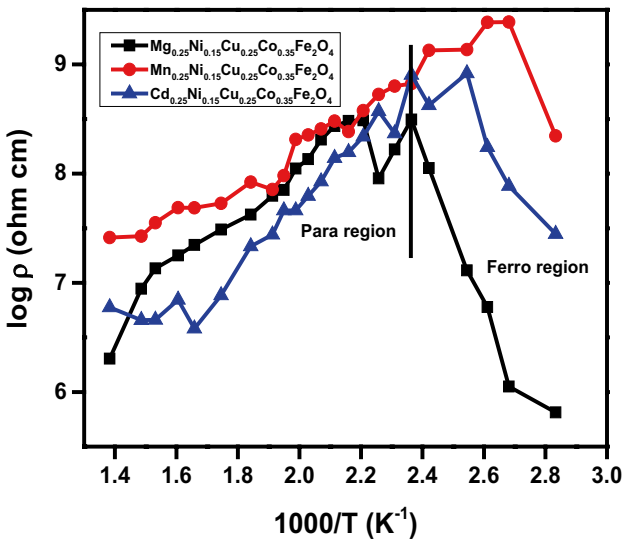

Fig. 8 Log of resistivity and 1000/T of M^{2+}-doped NCCF ferrites

frequency range from 4 Hz to 8 MHz. The ac conductivity has a direct relation with frequency as frequency increased and ac conductivity also increased (as seen in Fig. 6) which is a good match with Koops and Maxwell–Wagner's model [42].

3.5 UV–vis Spectroscopy

UV–vis spectra were used to investigate the optical characteristics of M^{2+}-doped NCCF ferrites in the range of 200 to 800 nm. Equation (26) was used to find the absorption coefficient of the prepared ferrites as given [28]:

$$\alpha = 1.303 log A \tag{26}$$

Here, A and α indicate the absorbance and absorbance coefficient respectively. The following Tauc's Eq. (27) [28] was used to determine the energy bandgap of the prepared ferrites:

$$\alpha h\nu = B(h\nu - E_g)^m \tag{27}$$

Here, m and B are the constants. h, ν, and E_g represent the Plank's constant, frequency of the incident photon, and the energy bandgap of the prepared ferrites. Figure 7 shows the optical energy band gap by plotting between $(\alpha\, h\nu)^2$ and $h\nu$ of the M^{2+} doped NCCF ferrites and observed in the range of 1.67 to 0.85 eV as listed in Table 5. The outcomes of the prepared ferrites revealed that the Cd^{2+}-doped ferrite has a low energy band gap as compared to Mg^{2+} and Mn^{2+}-doped ferrites.

3.6 Current–Voltage Measurements

DC resistivity depends on the composition and synthesized technique of the prepared ferrites which varied the distribution of cations at the tetrahedral and octahedral sites. The relation was used to find out resistivity [28]:

$$R = \frac{\rho L}{A} \tag{28}$$

Here, L is the thickness of the pellet, A is the area of the pellet, and ρ is the electric resistivity. Figure 8 shows the electric resistivity of the M^{2+}-doped NCCF ferrites with the addition of divalent metal ions at various temperatures. The higher exchange of charger carriers between Fe^{2+} and Fe^{3+} at the octahedral site reduced the electric resistivity. The calculated activation energy of the M^{2+}-doped NCCF ferrites reveals the resistivity nature of the ferrites. Equation (29) was used to the electric resistivity of the prepared ferrites as given [28]:

$$\rho = \rho_o exp\left(\frac{\Delta E}{k_B T}\right) \tag{29}$$

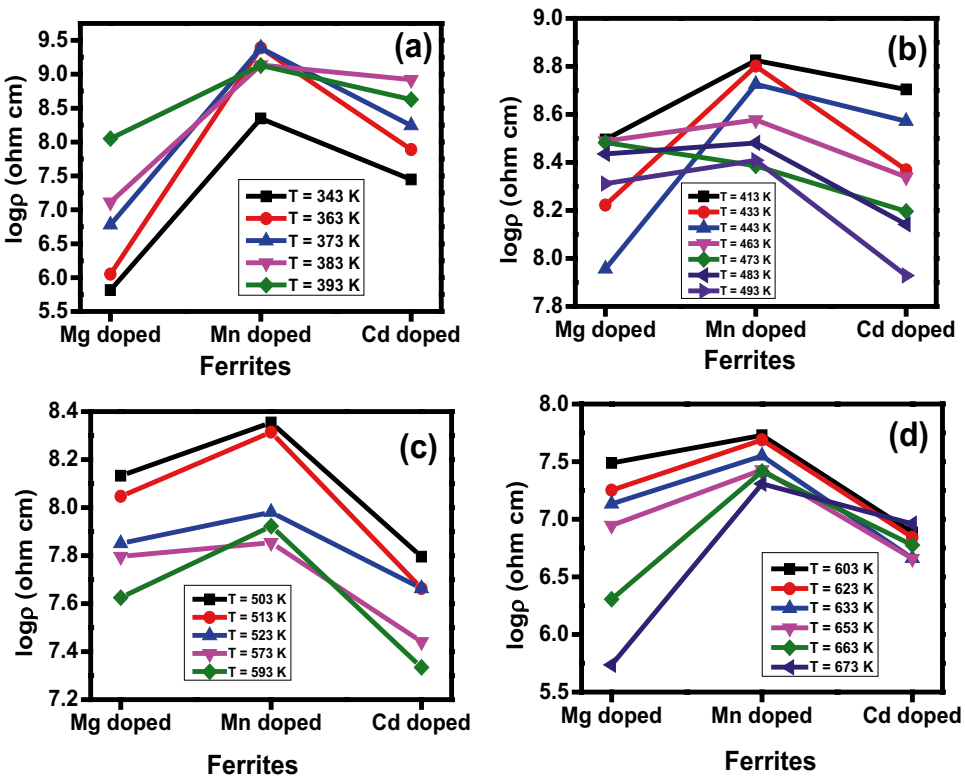

Fig. 9 Ferrites versus the log of resistivity of M^{2+}-doped NCCF ferrites

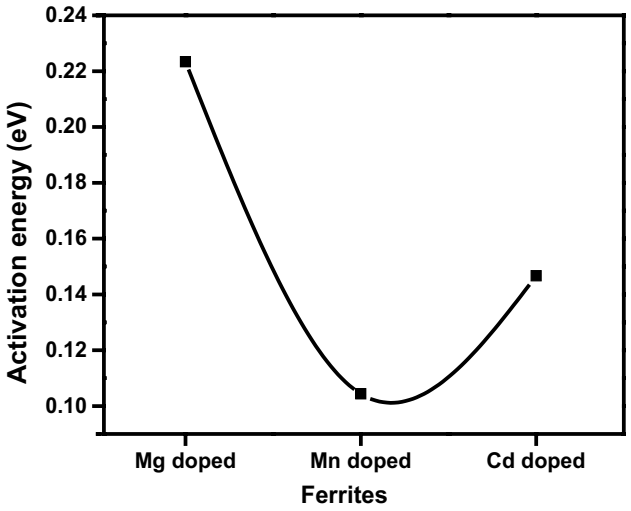

Fig. 10 Ferrites versus activation energy

Here, ρ, ρ_o, and ΔE are the electrical resistivity, temperature constant, and activation energy of the prepared ferrites respectively. k_B is the Boltzmann's constant. Figure 8 shows the electric resistivity measurements with 1000/T of the prepared ferrites. The obtained results have two regions in which the first region has the temperature range of 343 to 413 K, while the second region has the range above 413 K. It can be seen that the Mn^{2+}-doped ferrite has a high electrical resistivity while the Cd^{2+}-doped ferrite has a low value of electrical resistivity in the para region. The bending curves were divided into two-portion (ferromagnetic and paramagnetic) regions by kink points which indicated the transition temperature. These kink points revealed the variation of conductivity due to changing magnetic order from ferromagnetic region to paramagnetic region. The region below transition temperature is known as paramagnetic while the region above transition temperature is known as the ferromagnetic region. Figure 9 a, b, and c show the electrical resistivity of the Mn^{2+}-doped ferrite is high as compared to Mg^{2+} and Cd^{2+}-doped ferrites. Figure 10 shows the trend of activation energy for the as-prepared ferrites and the values are listed in Table 7. It was observed that the Mn^{2+} has a small value of activation energy as compared to Mg^{2+} and Cd^{2+}-doped ferrites.

Table 7 Activation Energy and transition temperature of M^{2+}-doped NCCF ferrites

Ferrites	Transition temperature (K)	Activation energy (eV)
Mg^{2+}-doped NCCF	411	0.2234
Mn^{2+}-doped NCCF	384	0.1046
Cd^{2+}-doped NCCF	412	0.1462

4 Conclusions

Sol–gel technique was employed to synthesize Mg^{2+}-, Mn^{2+-}, and Cd^{2+}-doped NCCF nanoparticles, and their cubic spinel structure was confirmed by the XRD analysis. The minimum lattice constant was 8.3664 Å while crystallite size decreased from 52.66 to 22.35 Å, and Mg^{2+}-doped NCCF ferrite has a maximum value of crystallite size. The variation in the upper and lower frequency bands of the M^{2+} doped NCCF ferrites indicates the distribution of cations at tetrahedral and octahedral sites which are also confirmed by Raman spectra. The minimum energy bandgap was 0.85 eV for Cd^{2+}-doped NCCF ferrite, and the maximum was 1.67 eV for Mg^{2+}-doped NCCF ferrite. The dielectric loss decreased with the substitution of divalent ions, and minimum dielectric loss was observed for Mg^{2+}-doped NCCF ferrite. Also, ac conductivity increased with an increasing applied frequency may be due to the large impedance. Mg^{2+}-doped NCCF ferrite has 0.2234 eV activation energy while Mn^{2+}-doped NCCF ferrite has 0.1046 eV activation energy. Hence, due to their incredible properties, Mg^{2+}-doped NCCF ferrite has potential applications in different fields.

Funding The Deanship of Scientific Research (DRS), King Khalid University, Abha, Saudi Aribia, funded this work through General Research Project, under grant no. R.G.P.1. 43/42.

References

1. Kefeni, K.K., Msagati, T.A., Mamba, B.B.: Ferrite nanoparticles: synthesis, characterisation and applications in electronic device. Mater. Sci. Eng., B **215**, 37–55 (2017)
2. Fawzi, A.S., Sheikh, A., Mathe, V.: Structural, dielectric properties and AC conductivity of Ni(1–x)ZnxFe2O4 spinel ferrites. J. Alloy. Compd. **502**, 231–237 (2010)
3. Sivakumar, N., Narayanasamy, A., Greneche, J.M., Murugaraj, R., Lee, Y.: Electrical and magnetic behaviour of nanostructured $MgFe_2O_4$ spinel ferrite. J. Alloy. Compd. **504**, 395–402 (2010)
4. Kefeni, K.K., Mamba, B.B.: Photocatalytic application of spinel ferrite nanoparticles and nanocomposites in wastewater treatment. Sustain. Mater. Technol. **23**, e00140 (2020)
5. Tatarchuk, T., Naushad, M., Tomaszewska, J., Kosobucki, P., Myslin, M., Vasylyeva, H., Ścigalski, P.: Adsorption of Sr (II) ions and salicylic acid onto magnetic magnesium-zinc ferrites: isotherms and kinetic studies. Environ. Sci. Pollut. Res. **27**, 26681–26693 (2020)
6. Tatarchuk, T., Mironyuk, I., Kotsyubynsky, V., Shyichuk, A., Myslin, M., Boychuk, V.: Structure, morphology and adsorption properties of titania shell immobilized onto cobalt ferrite nanoparticle core. J. Mole. Liq. **297**, 111757 (2020)
7. Xiang, J., Chu, Y., Shen, X., Zhou, G., Guo, Y.: Electrospinning preparation, characterization and magnetic properties of cobalt–nickel ferrite ($Co_{1-x}Ni_xFe_2O_4$) nanofibers. J. Colloid Interface Sci. **376**, 57–61 (2012)

8. Hamdaoui, N., Azizian-Kalandaragh, Y., Khlifi, M., Beji, L.: Cd-doping effect on morphologic, structural, magnetic and electrical properties of $Ni_{0.6-x}Cd_xMg_{0.4}Fe_2O_4$ spinel ferrite ($0 \leq x \leq 0.4$). J. Alloys Comp. **803**, 964–970 (2019)
9. dos Santos Amarante, M., Júnior, E.d.O.S., de Lima, R.G.A., Lente, M.H., Machado, J.P.B., da Cunha Migliano, A.C., de Brito, V.L.O.: Sintering behavior and electromagnetic properties of a Ni–Co ferrite/NiO biphasic ceramic. Mater. Res. Exp. **6**, 076110 (2019)
10. Kumar, K., Loganathan, A.: Structural, electrical and magnetic properties of large ionic size Sr^{2+} ions substituted Mg-Ferrite nanoparticles. Mater. Chem. Phys. **214**, 229–238 (2018)
11. Warsi, M.F., Iftikhar, A., Yousuf, M.A., Sarwar, M.I., Yousaf, S., Haider, S., Aboud, M.F.A., Shakir, I., Zulfiqar, S.: Erbium substituted nickel–cobalt spinel ferrite nanoparticles: tailoring the structural, magnetic and electrical parameters. Ceram. Int. **46**, 24194–24203 (2020)
12. Almessiere, M., Korkmaz, A.D., Slimani, Y., Nawaz, M., Ali, S., Baykal, A.: Magneto-optical properties of rare earth metals substituted Co-Zn spinel nanoferrites. Ceram. Int. **45**, 3449–3458 (2019)
13. Sadaqat, A., Almessiere, M., Slimani, Y., Guner, S., Sertkol, M., Albetran, H., Baykal, A., Shirsath, S.E., Ozcelik, B., Ercan, I.: Structural, optical and magnetic properties of Tb^{3+} substituted Co nanoferrites prepared via sonochemical approach. Ceram. Int. **45**, 22538–22546 (2019)
14. Almessiere, M., Ünal, B., Slimani, Y., Korkmaz, A., Baykal, A., Ercan, I.: Electrical properties of La^{3+} and Y^{3+} ions substituted $Ni_{0.3}Cu_{0.3}Zn_{0.4}Fe_2O_4$ nanospinel ferrites. Results Phys. **15**, 102755 (2019)
15. Slimani, Y., Unal, B., Almessiere, M., Korkmaz, A.D., Shirsath, S.E., Yasin, G., Trukhanov, A., Baykal A.: Investigation of structural and physical properties of Eu^{3+} ions substituted $Ni_{0.4}Cu_{0.2}Zn_{0.4}Fe_2O_4$ spinel ferrite nanoparticles prepared via sonochemical approach. Results Phys, **17**, 103061 (2020)
16. Aslam, A., Rehman, A.U., Amin, N., un Nabi, M.A., ul ain Abdullah, Q., Morley, N., Arshad, M.I., Ali, H.T., Yusuf, M., Latif, Z.: Lanthanum doped $Zn_{0.5}Co_{0.5}La_xFe_{2-x}O_4$ spinel ferrites synthesized via co-precipitation route to evaluate structural, vibrational, electrical, optical, dielectric, and thermoelectric properties. J. Phys. Chem. Solids **154**, 110080 (2021)
17. ALIa, I., Amin, N., Rehman, A., Akhtar, M., Fatima, M., Mahmood, K., ALIa, A., Mustafa, G., Hasan, M., Bibi, A.: Electrical and magnetic properties of $BaCo_xCd_{2-x}Fe_{16}O_{27}$ W-type hexaferrites ($0 \leq x \leq 0.5$). Digest J. Nanomater.Biostruct. **15**, (2020).
18. Amin, N., Hasan, M. S. U.,. Majeed, Z., Latif, Z., un Nabi, M. A.,. Mahmood, K., Ali, A., Mehmood, K., Fatima, M., Akhtar, M.: Structural, electrical, optical and dielectric properties of yttrium substituted cadmium ferrites prepared by Co-Precipitation method. Ceramics Internl. **46**, 20798–20809 (2020)
19. Amin, N., Akhtar, M., Sabir, M., Mahmood, K., ALIa, A., Mustafa, G., Hasan, M., Bibi, A., Iqbal, M., Iqbal, F.: Synthesis, structural and optical properties of Zn-substituted Co W-ferrites by coprecipitation method. J. Ovonic Res. **16**, 11–19 (2020)
20. Hussain, K., Amin, N., Arshad, M. I.: Evaluation of structural, optical, dielectric, electrical, and magnetic properties of Ce^{3+} doped $Cu_{0.5}Cd_{0.25}Co_{0.25}Fe_{2-x}O_4$ spinel nano-ferrites. Ceramics Internatl. **47**, 3401–3410 (2021)
21. Ali, H.T., Ramzan, M., Arshad, M.I., Morley, N.A., Abbas, M.H., Yusuf, M., Rehman, A.U., Mahmood, K., Ali, A., Amin, N.: Tailoring the optical, and magnetic properties of La-BaM hexaferrites by Ni substitution. Chin. Phys. B (2021). https://doi.org/10.1088/1674-1056/ac1412
22. Rehman, A. U., Morley, N., Amin, N., Arshad, M.I., un Nabi, M.A., Mahmood, K., Ali, A., Aslam, A., Bibi, A., Iqbal, M.Z.: Controllable synthesis of La^{3+} doped $Zn_{0.5}Co_{0.25}Cu_{0.25}Fe_{2-x}La_xO_4$ (x = 0.0, 0.0125, 0.025, 0.0375, 0.05) nano-ferrites by sol-gel auto-combustion route. Ceramics Internatl. **46**, 29297–29308 (2020)
23. Kale, A., Gubbala, S., Misra, R.: Magnetic behavior of nanocrystalline nickel ferrite synthesized by the reverse micelle technique. J. Magn. Magn. Mater. **277**, 350–358 (2004)
24. Shirsath, S.E., Toksha, B., Jadhav, K.: Structural and magnetic properties of In^{3+} substituted $NiFe_2O_4$. Mater. Chem. Phys. **117**, 163–168 (2009)
25. Rehman, A.U., Amin, N., Tahir, M.B., un Nabi, M.A., Morley, N., Alzaid, M., Amami, M., Akhtar, M., Arshad, M.I.: Evaluation of spectral, optoelectrical, dielectric, magnetic, and morphological properties of RE^{3+} (La^{3+}, and Ce^{3+}) and Co^{2+} co-doped $Zn_{0.75}Cu_{0.25}Fe_2O_4$ ferrites. Mater. Chem. Phys. 125301 (2021)
26. Aslam, A., Morley, N., Amin, N., Arshad, M.I., un Nabi, M. A., Ali, A., Mahmood, K., Bibi, A., Iqbal, F., Hussain, S.: Study of structural, optical and electrical properties of La^{3+} doped $Mg_{0.25}Ni_{0.15}Cu_{0.25}Co_{0.35}Fe_{2-x}La_xO_4$ spinel ferrites. Phys. B: Condensed Matter. **602**, 412565 (2021)
27. Amin, N., Razaq, A., Rehman, A. U., Hussain, K., Nabi, M., Morley, N., Amami, M., Bibi, A., Arshad, M.I., Mahmood, K.: Transport properties of Ce-doped Cd ferrites CdFe2− xCexO4. J. Superconduct. Novel Magnet. 1–11 (2021)
28. Hussain, K., Bibi, A., Jabeen, F., Amin, N., Mahmood, K., Ali, A., Iqbal, M.Z., Arshad, M.: Study of structural, optical, electrical and magnetic properties of Cu^{2+} doped $Zn_{0.4}Co_{0.6x}Ce_{0.1}Fe_{1.9}O_4$ spinel ferrites. Physica B: Condensed Matter. **584**, 412078 (2020)
29. Aslam, A., Razzaq, A., Naz, S., Amin, N., Arshad, M.I., Nabi, M.A.U., Nawaz, A., Mahmood, K., Bibi, A., Iqbal, F.: Impact of lanthanum-doping on the physical and electrical properties of cobalt ferrites. J. Superconduct. Novel Magnet. 1–10 (2021)
30. Javed Iqbal, M., Ahmad, Z., Meydan, T., Melikhov, Y.: Physical, electrical and magnetic properties of nano-sized Co-Cr substituted magnesium ferrites. J. Appl. Phys. **111**, 033906 (2012)
31. Zakir, R., Iqbal, S.S., Rehman, A.U., Nosheen, S., Ahmad, T.S., Ehsan, N., Inam, F.: Spectral, electrical, and dielectric characterization of Ce-doped Co-Mg-Cd spinel nano-ferrites synthesized by the sol-gel auto combustion method. Ceram. Int. **47**, 28575–28583 (2021)
32. Gabal, M., El-Shishtawy, R.M., Al Angari, A.: Structural and magnetic properties of nano-crystalline Ni–Zn ferrites synthesized using egg-white precursor. J. Magnet. Magnetic Mater. **324**, 2258–2264 (2012)
33. Nabi, M.A.U., Moin, M., Hasan, M., Arshad, M., Bibi, A., Amin, N., Mahmood, K., Ali, S.: Study of electrical transport properties of cadmium-doped Zn–Mn soft ferrites by co-precipitation method. J. Superconduct. Novel Magnet. 1–10 (2020)
34. Prasad, B.V., Babu, B.R., Prasad, M.S.R.: Structural and dielectric studies of Mg^{2+} substituted Ni–Zn ferrite. Mater. Sci.-Pol. **33**, 806–815 (2015)
35. Zeeshan, T., Anjum, S., Iqbal, H., Zia, R.: Substitutional effect of copper on the cation distribution in cobalt chromium ferrites and their structural and magnetic properties, Materials Science. Poland **36**, 255–263 (2018)
36. Jadhav, S.S., Shirsath, S.E., Toksha, B., Patange, S., Shukla, S., Jadhav, K.: Structural properties and cation distribution of Co–Zn nanoferrites. Int. J. Mod. Phys. B **23**, 5629–5638 (2009)
37. Abdallah, H.M., Moyo, T., Ngema, N.: The effect of temperature on the structure and magnetic properties of $Co_{0.5}Ni_{0.5}Fe_2O_4$ spinel nanoferrite. J. Magnet. Magnetic Mater. **394**, 223–228 (2015)
38. Yadav, R.S., Kuřitka, I., Havlica, J., Hnatko, M., Alexander, C., Masilko, J., Kalina, L., Hajdúchová, M., Rusnak, J., Enev, V. : Structural, magnetic, elastic, dielectric and electrical properties of hot-press sintered $Co_{1-x}Zn_xFe_2O_4$ (x = 0.0, 0.5) spinel ferrite nanoparticles. J. Magnet. Magnetic Mater. **447**, 48–57 (2018)

39. Issa, B., Obaidat, I.M., Albiss, B.A., Haik, Y.: Magnetic nanoparticles: surface effects and properties related to biomedicine applications. Int. J. Mol. Sci. **14**, 21266–21305 (2013)
40. Rahaman, M.D., Nahar, K., Khan, M., Hossain, A.A.: Synthesis, structural, and electromagnetic properties of $Mn_{0.5}Zn_{0.5-x}Mg_xFe_2O_4$ (x = 0.0, 0.1) polycrystalline ferrites, Physica B: Condensed Matter, **481**, 156–164 (2016)
41. Thakur, A., Mathur, P., Singh, M.: Study of dielectric behaviour of Mn–Zn nano ferrites. J. Phys. Chem. Solids **68**, 378–381 (2007)
42. Ajmal, M., Islam, M.U., Ashraf, G.A., Nazir, M.A., Ghouri, M.: The influence of Ga doping on structural magnetic and dielectric properties of $NiCr_{0.2}Fe_{1.8}O_4$ spinel ferrite, Physica B: Condensed Matter, **526**, 149–154 (2017)